Large Eddy Simulation and Study of the Urban Boundary Layer

MIAO Shiguang*[1,2] (苗世光) and JIANG Weimei[1] (蒋维楣)

[1] *Department of Atmospheric Sciences, Nanjing University, Nangjing* 210093

[2] *Institute of Urban Meteorology, China Meteorological Administration, Beijing* 100089

(Received 14 July 2003; revised 16 February 2004)

ABSTRACT

Based on a pseudo-spectral large eddy simulation (LES) model, an LES model with an anisotropy turbulent kinetic energy (TKE) closure model and an explicit multi-stage third-order Runge-Kutta scheme is established. The modeling and analysis show that the LES model can simulate the planetary boundary layer (PBL) with a uniform underlying surface under various stratifications very well. Then, similar to the description of a forest canopy, the drag term on momentum and the production term of TKE by subgrid city buildings are introduced into the LES equations to account for the area-averaged effect of the subgrid urban canopy elements and to simulate the meteorological fields of the urban boundary layer (UBL). Numerical experiments and comparison analysis show that: (1) the result from the LES of the UBL with a proposed formula for the drag coefficient is consistent and comparable with that from wind tunnel experiments and an urban subdomain scale model; (2) due to the effect of urban buildings, the wind velocity near the canopy is decreased, turbulence is intensified, TKE, variance, and momentum flux are increased, the momentum and heat flux at the top of the PBL are increased, and the development of the PBL is quickened; (3) the height of the roughness sublayer (RS) of the actual city buildings is the maximum building height (1.5–3 times the mean building height), and a constant flux layer (CFL) exists in the lower part of the UBL.

Key words: uniform underlying surface, urban boundary layer, planetary boundary layer, large eddy simulation (LES), anisotropy, turbulent kinetic energy closure model

1. Introduction

Among three modeling methods of the planetary boundary layer (PBL) (direct numerical simulation (DNS), Reynolds-average numerical simulation (RANS), large eddy simulation (LES), LES partly avoids the difficulty of finding a widely applicable subgrid scale (SGS) closure model in RANS, and is a compromise between the principle of DNS and the constraint of computation power. Two broad roles for LES in future PBL research are (Wyngaard, 1984): (1) Studying the sources and physics of the inherent uncertainty and quantifying it for applications, particularly in turbulent dispersion; (2) Generating databases for developing, designing, and validation of PBL models and SGS processes. Kosović and Curry (2000) simulated the stable boundary layer very well using an LES model with the nonlinear SGS model. Cai (1999) studied the characteristics of the convective boundary layer (CBL) over an idealized patchy urban surface using RAMS-LES. Miao and Jiang (2003) modeled the turbulent flow in a forest canopy and forest PBL with the aid of a pseudo-spectral LES model.

With the rapid increase of population and great economic development, the extent of urbanization becomes greater and greater. Consequently, more attention has been paid to the urban meteorological environment, which must be studied using a PBL numerical model with high resolution. Simultaneously, the complexity of the urban geographical environment, the effect of artificial activity, the multi-scale interaction of processes in the urban atmosphere, and the cross-sphere interactions caused by urban water-soil-air-biology, combine and keep interacting mutually, bringing huge difficulties and challenges to the research.

Brown (2000) summarized the urban parameterization for mesoscale meteorological models. There are three methods to account for the bulk, or area-averaged, effects of urban buildings: the aerodynamic roughness length approach, the attenuation approach,

*E-mail: sgmiao@ium.cn; jwm@nju.edu.cn

and the drag approach. The first approach is applied easily but the horizontally-homogeneous condition used in the Monin-Obukhov (M-O) similarity theory is not satisfied within and for some distance above the urban canopy. The attenuation approach needs many observation data and parameters which are hard to obtain. The drag approach incorporates drag terms into the model, so the effects of the canopy can be applied to the flow interior. Roth (2000) reviewed atmospheric turbulence over cities, and concluded that the extreme heterogeneity of urban surfaces, usually at all length scales, makes the definition of a uniform fetch impossible, and the results on integral statistics and spectra suggest the existence of strong similarities between turbulent flows over cities and plant canopies.

In this paper, based on the pseudo-spectral LES model of Moeng (1984), an LES model with the anisotropy SGS closure model and an explicit multistage third-order Runge-Kutta scheme is established. The modeling and analysis of the PBL with a uniform underlying surface under various stratifications are performed. Then, similar to the description of a forest canopy, the application of LES to the research of the urban boundary layer (UBL) is studied and a comparison with the results from wind tunnel experiments and an urban subdomain scale numerical model is performed, which meet two key problems (parameter specification and validation) in the urban parameterization for mesoscale meteorological models.

2. LES model

The equations of Moeng's (1984) LES model consist of the continuity equation, momentum equation, and thermodynamic equation with the TKE closure model (Deardorff, 1980). The equations are discretized by a pseudo-spectral method with Fourier transforms in the homogeneous directions, x and y, and second-order finite differences in the vertical direction (z). The boundary conditions at the surface are constructed using M-O similarity theory, while a radiation condition is applied at the upper boundary; periodic boundary conditions are applied in both the x and y directions.

In order to simulate the PBL under various stratifications, the anisotropy TKE closure model (Sullivan et al., 1994) and a third-order Runge-Kutta scheme (Ge, 1994; Zhang and Shen, 2003) is introduced into this model. The anisotropy TKE closure model improves on the TKE closure model by aiming at the low resolution near the surface and the effect on SGS stresses by mean shear. The SGS stresses are split into what are termed the isotropic and inhomogeneous contributions. The isotropic eddy viscosity depends on the magnitude of the fluctuating strain rate, while the inhomogeneous term varies with the magnitude of the mean strain rate. When using this SGS model, the effect of mean shear is subtracted from the production term in the SGS TKE equation.

3. LES of PBL with a uniform underlying surface

3.1 *LES of the convective boundary layer* (*CBL*)

Two CBL cases are run with different SGS models, and the parameters are listed in Table 1. Here, D80 and S94 represent the TKE model and anisotropy TKE model respectively; Q_s, U_g, L, Z_i, w_*, and t_* are the surface heat flux, geostrophic wind speed, M-O length, the height of CBL, velocity scale, and time scale respectively.

The initial conditions of the two cases are: (1) The potential temperature below 800 m is 300 K, the lapse rate above 800 m is 0.003 K m^{-1}; z_0=0.1 m; the latitude is 73°N; (2) In order to start turbulence, a stochastic perturbation of temperature (with an amplitude of 0.1 K) and velocity (with an amplitude of 0.5 m s^{-1}) is introduced into the 4 levels above ground.

Figure 1 is the heat flux profile of cases LESC4 and LESC5. Figure 1a shows that the value and the variation with height of the heat flux from our LES agrees very well with the LES result of Schmidt and Schumann (1989) and the observational data. The heat flux varies linearly with height in CBL: it decreases with the increase of height above ground, is negative from the height of $Z \sim 0.85Z_i$, reaches the negative extreme at $Z \sim Z_i$, then increases to zero at the height of $1.15Z_i$. The negative zone of heat flux at the top of CBL indicates the transportation of heat from the above air by the entrainment.

Table 1. Parameters of LES cases of CBL.

Case name	Domain size (km×km×km)	Grid ($X \times Y \times Z$)	SGS Model	Q_s (K m s^{-1})	U_g (m s^{-1})	L (m)	Z_i (m)	w_* (m s^{-1})	t_* (s)
LESC4	10.24×10.24×2	128×128×40	S94	0.1	5.0	–28.1	1200	1.58	761
LESC5	10.24×10.24×2	128×128×40	D80	0.1	5.0	–25.0	1250	1.60	782

Table 2. Parameters of LES cases of NBL.

Case name	Domain size	Grid	SGS	Q_s	U_g	$Z_i \to h$	$w_* \to u_*$	t_*
name	(km×km×km)	$X \times Y \times Z$	Model	(K m s^{-1})	(m s^{-1})	(m)	(m s^{-1})	(s)
LESN1	2×2×1	96×96×96	S94	0.05→ 0	5.0	719→ 629	1.06→ 0.223	678→ 2700
LESN2	2×2 × 1	96×96 × 96	D80	0.05→ 0	5.0	750→ 564	1.07→ 0.222	701→ 2541

Note: The values on the two sides of "→" represent the values of CBL and NBL respectively.

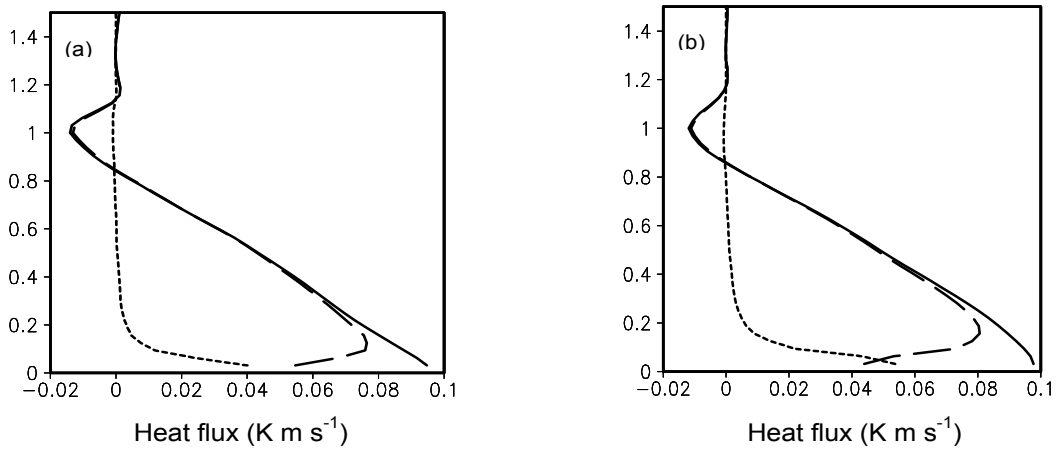

Fig. 1. The profile of heat flux (solid line total, dashed line resolved, short dashed line SGS): (a) Case LESC4; (b) Case LESC5.

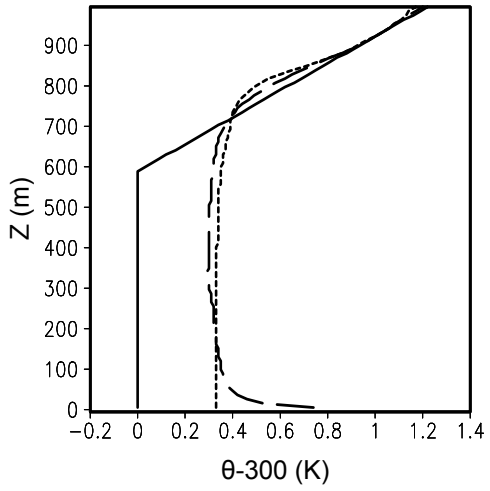

Fig. 2. Horizontal mean profile of potential temperature of case LESN1 (solid, dashed, short dashed lines are $t = 0, t = 6t_*$ (CBL), $t = 6t_*$ (NBL) respectively).

We can see from the comparison between Fig. 1a and Fig. 1b that, above the surface layer, the heat flux profiles from the two cases are very similar. In the surface layer, the contribution of the SGS heat flux to the total part in adopting the anisotropy TKE closure model is smaller than that in adopting the TKE closure model, and the contribution of the resolved part of the one is bigger than the other, which meets the requirement of LES. The profiles of TKE and vertical momentum flux are analogous (figures omitted). Because in the anisotropy TKE closure model the production term of SGS TKE by mean shear is added into the SGS stress, then in the surface layer the SGS TKE decreases and the resolved TKE increases.

3.2 *LES of the neutral boundary layer* (*NBL*)

Similar to the modeling method of NBL by Moeng and Sullivan (1994), we set the surface heat flux to Q_s=0.05 m s^{-1} K, integrate the LES model for $6t_*$, and thus the quasi-steady CBL is obtained; then, we change Q_s to zero, integrate the LES model for another $6t_*(t_* = h/u_*)$ ($t_* = h/u_*, u_*$ is friction velocity) and the quasi-steady NBL is achieved. Two NBL cases are run with different SGS models, and the parameters are listed in Table 2.

The initial conditions of the two cases are: The potential temperature below 600 m is 300 K, the lapse rate above 600 m is 0.003 K m^{-1}; z_0=0.1 m; the latitude is 73°N; In order to start turbulence, a stochastic perturbation of temperature (with an amplitude of 0.1 K) and velocity (with an amplitude of 0.5 m s^{-1}) is introduced into the four levels above ground.

Figure 2 presents the horizontal mean profile of potential temperature of case LESN1. We can see that in

the middle-lower part of the NBL, the potential temperature is approximately the same; in the upper part there is a weak inversion; at the top, there is a strong covering inversion. Comparing the two profiles of NBL and CBL, the temperature decreases in the lower part of the NBL, near the surface the decrease is especially distinct; the temperature increases in the upper part; so the temperature in the whole NBL reaches a uniform distribution. At the top of the NBL, the entrainment transports the heat downwards from the above inversion layer, so the temperature of the inversion layer decreases and the temperature in the upper part of the NBL increases.

In Fig. 3, snapshots of the $U-\langle U\rangle$ and W flow fields in the $X-Y$ plane at a single vertical location well within the surface layer, $Z/h = 0.07$, for case LESN1 and case LESN2 are shown (here, U and W are component of wind speed on X and Y direction respectively, $\langle U\rangle$ represents the horizontal mean of U). The shading and contouring scheme is selected to highlight the areas of maximum and minimum intensities in each field. It shows that the alignment of the streaky structures are apparent in all of the flow variables examined, but are especially visible in the plots of the u horizontal fluctuations. The streaks are roughly aligned with the mean flow direction. At the same time, the regions where positive (negative) W fluctuations occur are aligned with negative (positive) U fluctuations. These structures resemble the often observed streaks in flat plate boundary layers, and are similar to the flow patterns observed in numerical simulations of channel flow. Inspection of the figures reveals that the streaky structures of case LESN1 are more detailed than those of case LESN2. Because of the increase of the resolved part when adopting anisotropy TKE closure, the more energetic higher frequency motions are modeled.

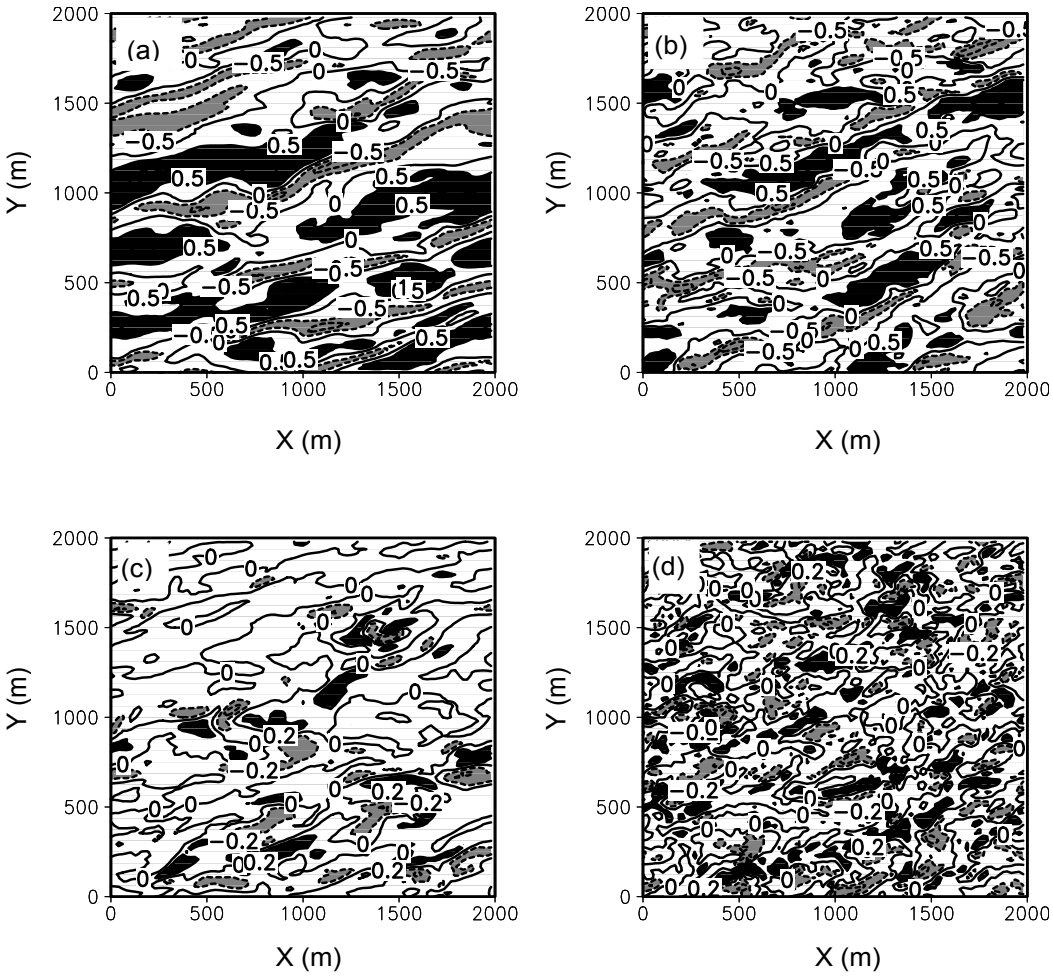

Fig. 3. Contours of case LESN1 (right side) and case LESN2 (left side) at the height of $Z/h = 0.07$: top $U - \langle U\rangle$ field, bottom W field. $U - \langle U\rangle$ contours (–1, –0.5, 0, 0.5, 1), dark (light) shaded values are larger (smaller) than 0.5 (–0.5); W contours (–0.4, –0.2, 0, 0.2, 0.4); dark (light) shaded values are larger (smaller) than 0.2 (–0.2).

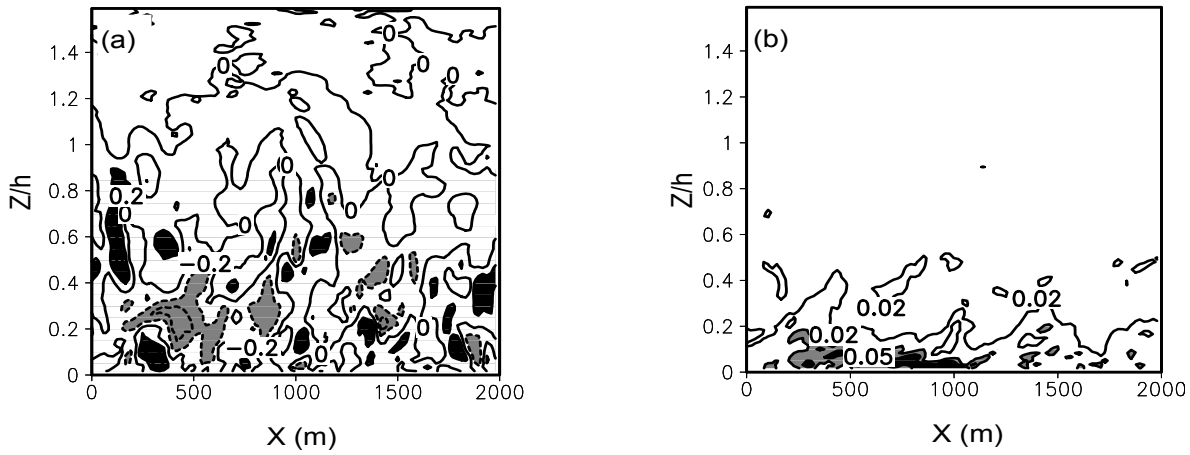

Fig. 4. Contours of case LESN1 at $Y = 60\Delta Y$: (a) W, contours (–0.4,–0.2, 0, 0.2, 0.4), dark (light) shaded values are larger (smaller) than 0.2 (–0.2); (b) e, contours (0.02, 0.05, 0.08), dark (light) shaded values are larger than 0.08 (0.05).

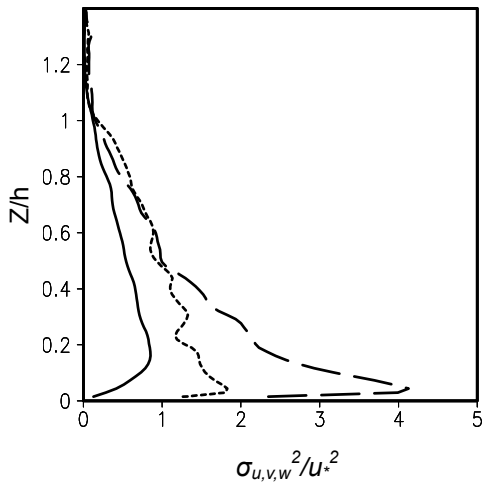

Fig. 5. Profiles of the velocity variances from case LESN1 (dashed, short dashed and solid lines are $\sigma_u^2/u_*^2, \sigma_v^2/u_*^2$, and σ_w^2/u_*^2 respectively).

Figures of $U-\langle U\rangle$ and W in the $X-Y$ plane of case LESN1 at $Z/h = 0.15, 0.5, 0.8$ (omitted) show that the streaky structures, so readily visible at $Z/h = 0.15$, gradually disappear with increasing Z; and by about $Z/h = 0.5$, the streaks are no longer distinguishable, having been replaced with spatially less coherent structures.

Noticeable features of the $X - Z$ views (Fig. 4) are the presence of numerical small eddy structures, which most often occur in updraft-downdraft pairs. This contrasts considerably with the few but very large updrafts present in the CBL. The structures in the CBL generally span the entire vertical extent of the domain, while in the NBL the structures tend to be concentrated below $0.8h$ at scales roughly one-half of h. The SGS TKE is bigger near the surface, and gradually decreases with increasing Z.

Figure 5 gives the profiles of the velocity variances. We can find that in NBL the velocity variances increase smoothly and reach the maximum at $Z/h = 0.05 - -0.15$ followed by a gradual decrease with height, and $\sigma_u^2/u_*^2 > \sigma_v^2/u_*^2 > \sigma_w^2/u_*^2$ (σ_i^2 represents the velocity variance on i direction). It should be noted that Mason and Thomson (1992) obtained the vertical profiles of the velocity variances similar to that from our LES model after the introduction of stochastic backscatter closure model.

3.3 *LES of the stable boundary layer* (*SBL*)

Similar to the modeling method of SBL by Kosović and Curry (2000), we adopt the measurement made during the Beaufort Sea Arctic Stratus Experiment (BASE) on 1 October 1994 from flight number 7 as the initial condition; the quasi-steady SBL is obtained by running the LES model for 12 hours of physical time (corresponds to $6/f$ where f is the Coriolis parameter). The domain size and grid number of case LESS1 are 400 m×400 m×300 m and 48×48×40 respectively. The other parameters are listed in Table 3.

Figure 6 shows the potential temperature profiles of SBL. The result of our LES model is consistent with the measurement and the LES of Kosović and Curry (2000) using the nonlinear SGS model, and has the same law of vertical distribution via the observation by Nieuwstadt (1984). There are four layers in a quasi-steady SBL: (1) the surface layer with a strong inversion: 0–0.1h; (2) the central layer where turbulence effects dominate: 0.1–0.8h; (3) the elevated inversion layer that caps the SBL: 0.8–1h; (4) the overlying/environment inversion: above 1h. But the defini-

Table 3. Parameters of LES cases of SBL.

Case name	Latitude	SGS Model	U_g (m s^{-1})	Surface cooling rate (K h^{-1})	Z_0 (m)	h (m)	L (m)	h/L	u_* (m s^{-1})	$1/f$ (h)
LESS1	73°N	S94	8	0.25	0.1	228.95	121.48	1.88	0.272	2.00

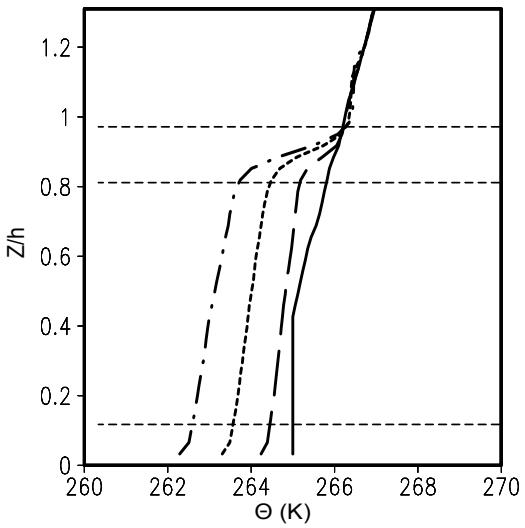

Fig. 6. The potential temperature profiles from case LESS1 (solid, dashed, short dashed, dotted-dashed lines are $t = 0, 2/f, 4/f, 6/f$ respectively).

tion of the SBL top differs between Kosović and us: Kosović defines

$$h = \frac{Z|_{\langle uw\rangle = 0.05u_*^2}}{0.95},$$

the height at which $\langle uw\rangle$ (vertical momentum flux) vanishes. We define

$$h = \frac{Z|_{u_{*l}^2 = 0.05u_*^2}}{0.95},$$

the height at which the turbulent stress vanishes and unequivocally defines the boundary between turbulent and nonturbulent layers.

Figure 7 presents contours of $U - \langle U\rangle$ and W in the $X - Y$ plane at $Z/h = 0.13$. It shows that a few small streaky-like structures develop in the SBL, especially visible in the plots of the u horizontal fluctuations, roughly aligned with the mean flow direction. And the regions where negative U fluctuations occur are aligned with positive W fluctuations, negative θ fluctuations, and big TKE (figures omitted).

The slice of W at $Y = 10\Delta Y$ (grid spacing on Y direction) (Fig. 8) reveals that smaller sized structures develop in the SBL, and there are some updraft/downdraft pairs. The eddies form at scales closer to $h/4$, and there are more horizontal eddies than vertical ones. Although the pattern of the eddies appears patchy, their production is continuous. This is contrary to what we would expect for turbulence that is globally intermittent. There are more eddies below $0.5h$ and less eddies above $0.5h$.

In Fig. 9, we present the Ekman spiral of quasi-steady wind profiles for case LESS1. The angle between the low-level wind vector and the geostrophic wind vector is approximately 35.5° which is close to the 30° of Kosović and Curry (2000), bigger than the 24° from our LES of NBL, smaller than the 45° of the classic Ekman spiral, and much smaller than the 60° predicted by Nieuwstadt's model. The maximum of supergeostrophic wind, 11%, appears at Z/h=0.83. While the Brunt-Väisälä frequency defined as

$$N = \left(\frac{g}{\theta_0}\frac{\partial\langle\theta\rangle}{\partial Z}\right)^{1/2}$$

reaches the maximum, 0.06Hz, at $0.88h$. θ is potential temperature, and θ_0 is the initial value of θ. So any waves that propagate vertically upward from below have frequencies smaller that 0.06 Hz. The acceleration by the inertia fluctuation and the inhibition of turbulence form the supergeostrophic wind (low level jet). Thus the maximum value of the wind speed in the inversion is the inherent characteristic of the quasi-steady SBL.

We know from case LESS2, which uses the TKE closure model (Deardorff, 1980) (the other parameters are the same as case LESS1), that it cannot produce the correct characteristics of the SBL including the profile of potential temperature. So the LES model adopting TKE closure cannot be applied to the simulation of the SBL.

4. LES of UBL

4.1 *The description of the urban building canopy in LES*

Similar to the description of a forest canopy in LES (Miao and Jiang, 2003) and the urban parameterizations of a building canopy for mesoscale meteorological models (Brown, 2000), the drag term on momentum and the production term of TKE by subgrid city buildings are introduced to the LES equations to account for the area-averaged effect of the subgrid urban canopy elements (here, for simplification, the dynamical effect of the buildings is considered but the thermal effect is excluded):

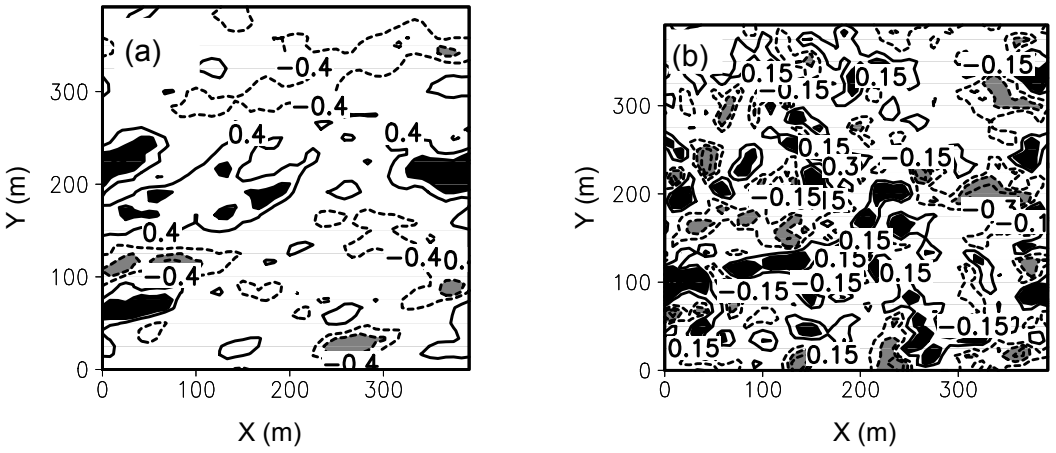

Fig. 7. Contours of case LESS1 at the height of $Z/h = 0.13$: (a) $U - \langle U \rangle$, contours (–1.2, –0.8, –0.4, 0, 0.4, 0.8, 1.2), dark (light) shaded values are larger (smaller) than 0.8 (–0.8); (b) W, contours (–0.6, –0.45, –0.3, –0.15, 0.15, 0.3, 0.45, 0.6); dark (light) shaded values are larger (smaller) than 0.3 (–0.3).

$$\frac{\partial \overline{U}}{\partial t} = F_{\overline{U}} - C_{\rm db} A \overline{U} |\overline{U}| \,, \tag{1}$$

$$\frac{\partial \overline{V}}{\partial t} = F_{\overline{V}} - C_{\rm db} A \overline{V} |\overline{V}| \,, \tag{2}$$

$$\frac{\partial e}{\partial t} = F_e + C_{\rm db} A [|\overline{U}|^3 + |\overline{U}|^3] \,. \tag{3}$$

Here, $\overline{U}$ and $\overline{V}$ are the average wind speed on X and Y direction respectively; e represents TKE. $F_{\overline{U}}, F_{\overline{V}}, F_e$, are the original right terms of their respective equations; $C_{\rm db}$ is the drag coefficient of urban buildings; A (a function of the height) is the building area density, i.e. the surface area of the buildings that is perpendicular to the wind per unit volume of the urban canopy. So the drag force will be non-zero within the canopy and will "turn-off" at some height above the canopy in response to the building area density A term.

We can see that the drag force in the momentum equations and the turbulent production term in the TKE equation are linearly dependent on the magnitude of the drag coefficient $C_{\rm db}$. Brown (2000) shows that $C_{\rm db}$ values range from 0.7 to 1.5 for buildings of different shapes and sizes. Although there should be dependence on number, spacing, height, and shape of buildings, as well as approach flow angle, Brown and Williams (1998) use an average value of 1.0 for all urban land use categories in their mesoscale meteorological modeling of UBL. Raupach (1992) obtains a $C_{\rm db}$ of 0.4 for cubic arrays of roughness elements in wind tunnel experiments. One might also expect that the drag coefficient will be smaller in regions where buildings are all about the same height, and be larger when building heights change relative to one another. So we define the drag coefficient as follows to include the effect by the distribution of the heights of subgrid buildings:

$$C_{\rm db} = 0.4 + \frac{\sigma_{\rm h}}{\overline{h}} \,, \tag{4}$$

where $\sigma_{\rm h}$ and $\overline{h}$ are the standard deviation and the average building height respectively.

The drag method has the advantage over the roughness length approach in that the effects of the buildings can be applied to the flow interior, not just as a boundary condition. So the model can account for the height variation of the wind and the turbulence within the building canopy.

4.2 *The comparison of LES of UBL with wind tunnel experiments and an urban subdomain scale model*

According to four wind tunnel experiments of the meteorological environment in FZ (a typical residential subdomain with tower buildings) of Beijing (Ouyang et al., 2003) (the conditions are listed in Table 4), we run the Urban Subdomain Scale Model (USSM) where the buildings are considered explicitly (Miao et al., 2002) and the LES model under the some conditions. The LES cases adopt the anisotropy TKE closure with the grid spacing of 400 m×400 m×10 m and the grid number of 32×32×80. In harmony with the wind tunnel experiment, the cases of USSM and LES are all in neutral stratification and exclude the Coriolis force. We run the LES model for 30 min of physical time consistent with USSM.

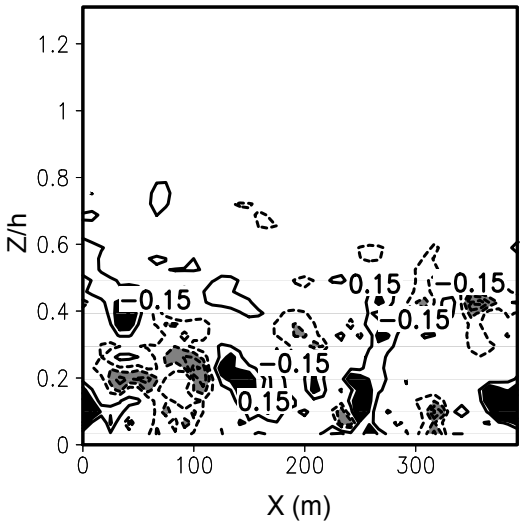

Fig. 8. Contours of W of case LESS1 at Y=10ΔY [contours: –0.6, –0.45, –0.3, 0, 0.3, 0.45, 0.6, dark (light) shaded values are larger (smaller) than 0.3 (–0.3)].

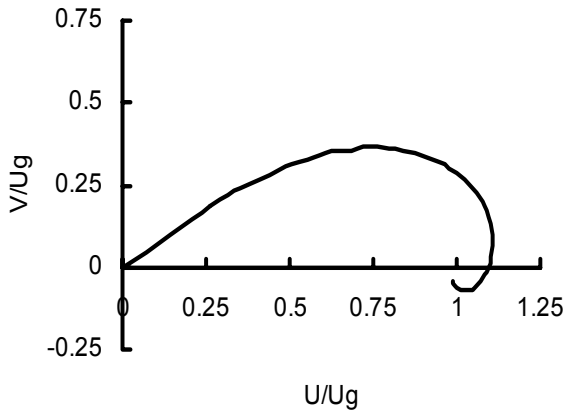

Fig. 9. Normalized Ekman spiral from case LESS1.

Figure 10 presents the vertical profiles of the mean building area density for all wind directions. In the FZ subdomain, there are many buildings below 10 m, and A decreases linearly above 20 m. Other parameters are listed in Table 5.

The profiles of mean wind speed and TKE from the wind tunnel experiment, USSM, and LES are compared in Fig. 11. We can see that the results from the wind tunnel experiment, USSM, and LES of UBL are consistent and comparable. Above 100 m, the profiles of mean the wind speed from wind tunnel experiment are small and do not match the power law of the wind profile, which may be caused by the apparatus and conditions of the wind tunnel. Below the maximum building height, the mean wind speed from USSM is smaller than that from the wind tunnel experiment.

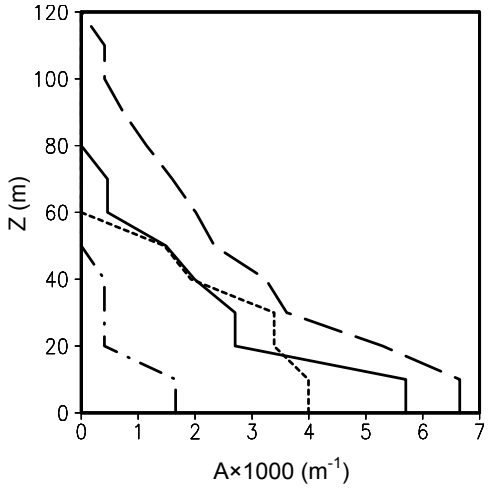

Fig. 10. The vertical profiles of the mean building area density of all wind directions (solid, dashed, short dashed, dotted-dashed lines are of FZ, JRJ, WKS1, WKS2, respectively).

Table 4. Conditions of wind tunnel experiments.

Experiment name	Initial wind direction	Initial wind speed (at the height of 10 m, in m s^{-1})
WT1	Southwest	1
WT2	Southwest	2
WT3	Northwest	1
WT4	Northwest	2

Table 5. Parameters of the four sub-domains.

Name	Area (m×m)	Maximum building height (m)	Mean building height (m)	Standard deviation of building height (m)	$C_{\rm db}$	The maximum of A×1000 (m^{-1})
FZ	460×660	78.0	25.2	18.6	1.14	6.34
JRJ	620×500	116.0	37.8	29.0	1.17	6.65
WKS1	650×650	50.0	36.4	11.8	0.72	3.99
WKS2	650×650	45.0	24.0	16.8	1.10	1.66

The small number of measurement points in the wind tunnel experiment and even less in the lower wind speed region near the buildings result in the difference. The wind profiles from LES agree well with those from USSM. The heights of the maximum TKES from the three methods are all about the maximum height of the buildings. But the maximum TKES from LES corresponding to cases WT1 and WT3 are bigger than those from USSM and the wind tunnel experiment.

4.3 *The analysis of the LES result of UBL*

Three LES cases of UBL are run with different subdomain parameters in neutral stratification, and the parameters are listed in Table 6. All three cases adopt the anisotropy TKE closure. u_* is calculated according to the maximum of vertical momentum flux. The subdomain parameters are shown in Table 5 and Figure 10, where JRJ, WKS1, and WKS2 are a business district, a sports area with dense buildings, and sports area with spare buildings, respectively.

The initial conditions of three cases are: The potential temperature below 600 m is 300 K, the lapse rate above 600 m is 0.005 K m^{-1}; U_g=8 m s^{-1}; z_0=0.05 m; The Coriolis force is excluded; In order to start tur-

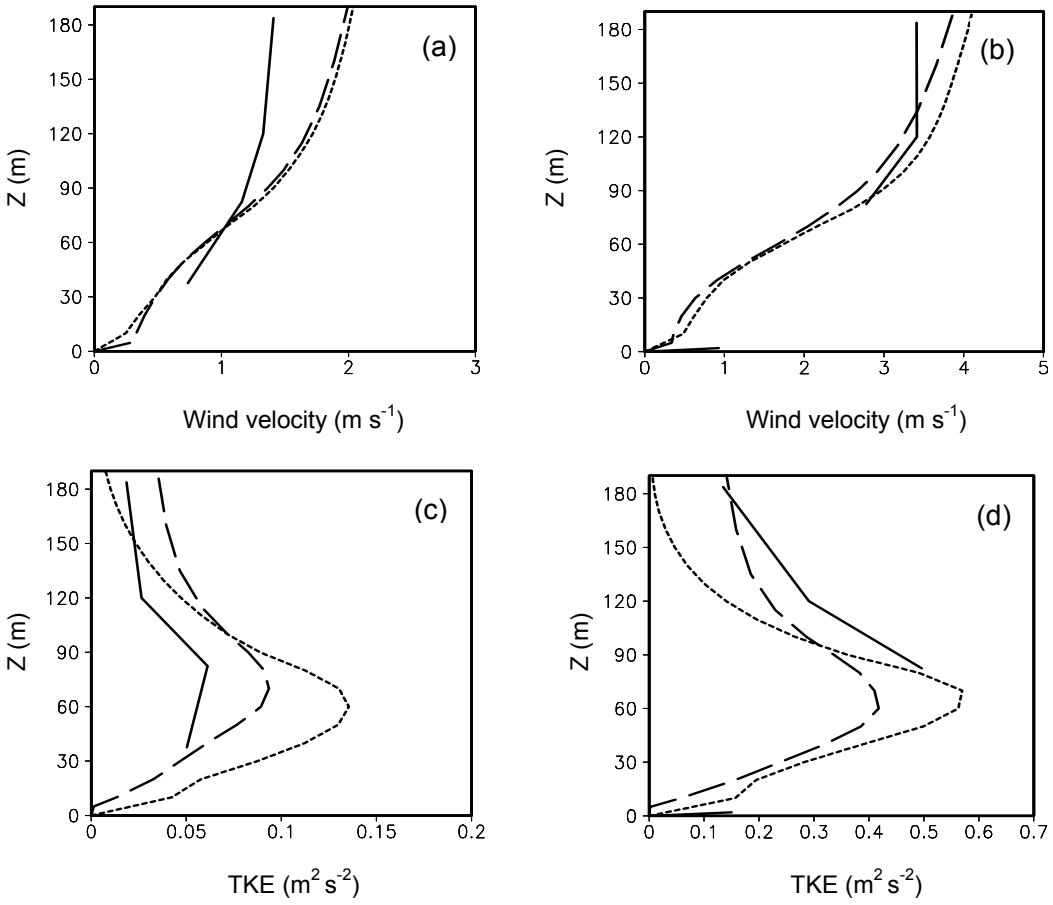

Fig. 11. The profiles of mean wind speed (top) and TKE (bottom): left side for WT1, right side for WT4; solid, dashed, and short dashed lines are from wind tunnel experiments, USSM, and LES, respectively.

Table 6. Parameters of LES cases of UBL.

Case name	Domain size (m×m×m)	Grid ($X \times Y \times Z$)	$A(z)$	h (m)	u_* (m s^{-1})	t_* (s)
LESU1	12800×12800×800	32×32×80	JRJ	700	0.364	1923.1
LESU2	12800×12800×800	32×32×80	WKS1	638.5	0.376	1698.1
LESU3	12800×12800×800	32×32×80	WKS2	600.0	0.218	2752.3

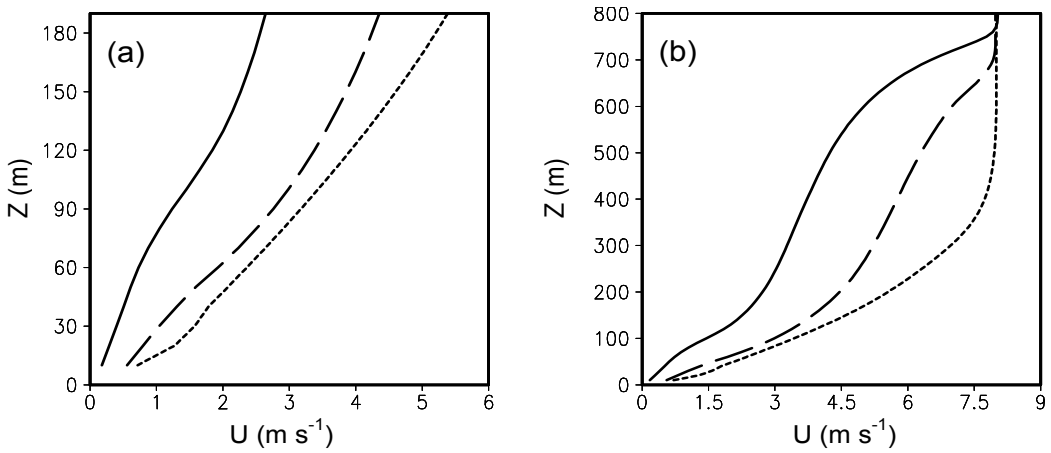

Fig. 12. The profiles of mean wind speed U of the three cases (solid, dashed, and short dashed lines are from cases LESU1, LESU2, and LESU3, respectively).

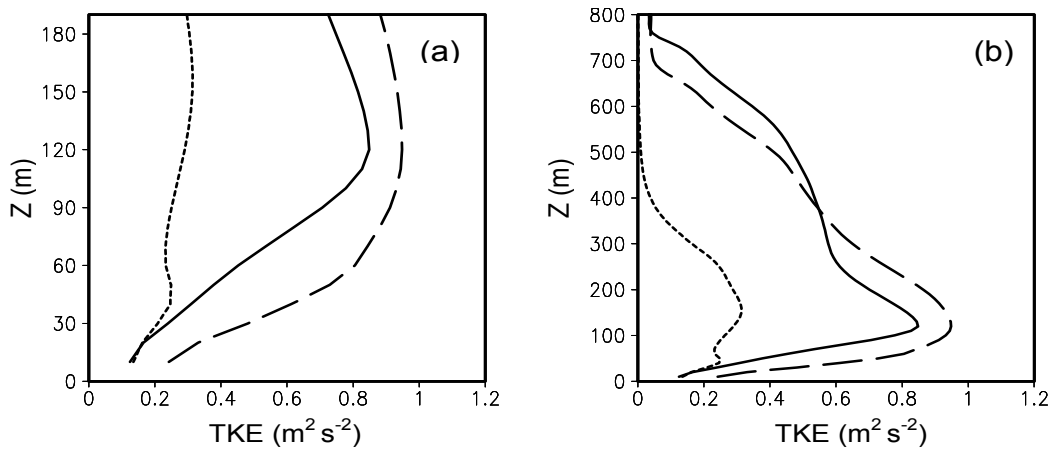

Fig. 13. The profiles of mean TKE for the same cases as in Fig. 12.

bulence, a stochastic perturbation of temperature (with an amplitude of 0.1 K) and velocity (with an amplitude of 0.5 m s^{-1}) is introduced into the four levels above ground.

The meteorological field at $6t_*$ is analyzed below.

Figure 12 gives the vertical profiles of the mean wind speed U of the three cases. Due to the drag by urban buildings, the wind speed in the building canopy and UBL decreases distinctly. The wind speed almost increases linearly with increasing Z in the canopy (approximately the maximum building height), and close to the logarithmic law above the canopy. So near the top of the building canopy the wind shear is very large. Inspection of the figures reveals that corresponding to the number and density of buildings in a subdomain, the wind speed in JRJ (WKS2) is smallest (largest).

Figure 13 shows the profiles of mean TKE from the three cases. TKE increases linearly with increasing Z from the ground and reaches the maximum just above the maximum building height, which matches the results from the modeling and experiment of a cubic obstacle. Among the three cases, the buildings in the JRJ subdomain are the densest, so the TKE is larger; the buildings in WKS1 are less dense, but the wind speed is larger than in JRJ, so the TKE is the largest; the buildings in WKS2 are sparse, so the TKE is small in the whole UBL.

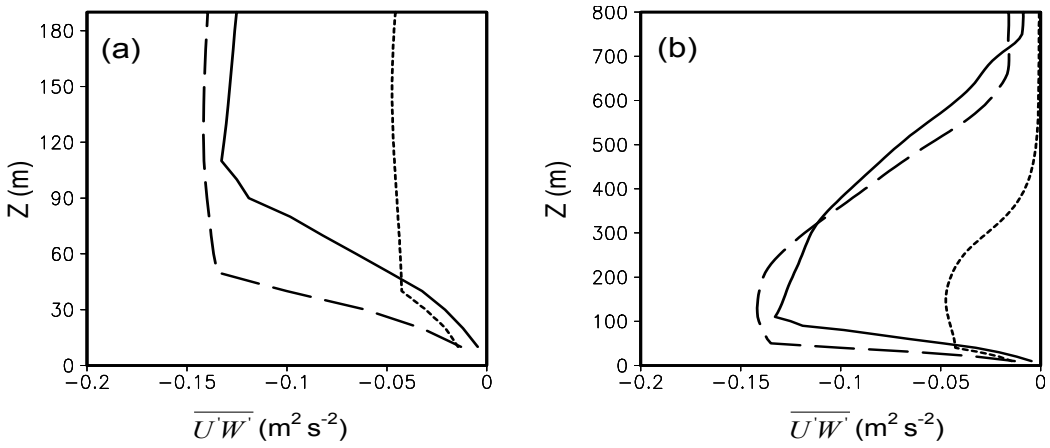

Fig. 14. The profiles of vertical momentum flux for the same cases as in Fig. 12.

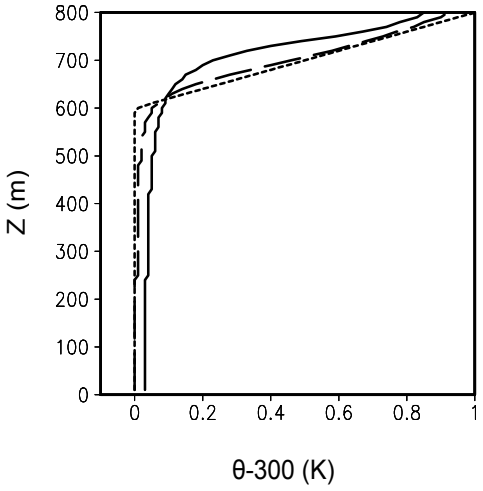

Fig. 15. The profiles of potential temperature for the same cases as in Fig. 12.

Figure 14 shows that vertical momentum flux varies linearly with height and reaches the maximum at the top of the building canopy (the maximum buiding height); consequently this layer is called the roughness layer (RS). From the top of the RS to about 200 m, the vertical momentum flux is almost constant; this layer is the constant flux layer (CFL). The relationship of three cases' values are similar to TKE.

Rotach (2001) gives the conceptual sketch of Reynolds stress in the PBL. The Reynolds stress reduction close to the roughness is due to form drag exerted on the flow by the building roughness elements.

Martilli et al. (2002) shows the vertical profiles of the normalized local friction velocity in a bidimensional case of an ideal city using a mesoscale model based on the finite volume method (FVM) adopting an urban surface exchange parameterization, including an average profile as obtained by Roth (2000) from a large number of full-scale observations. The comparisons among four results (LES, conceptual analysis, FVM mesoscale model, and observation) show that they agree very well in the structure of the UBL. Different from the plant canopy and buildings with the same height, the height of the RS of real urban buildings is the maximum building height (1.5–3 times the mean building height), and the CFL exists in the lower part of the UBL.

The profiles of potential temperature (Fig. 15) show that due to the increasing TKE and downward vertical heat flux by the building canopy, the temperature decreases in the entrainment layer and increases in the UBL, so it is a weak inversion in the upper part of the UBL. The urban building canopy quickens the development of the PBL.

5. Conclusion

The modeling and analysis of the PBL with a uniform underlying surface under various stratifications show the following. (1) The established LES model can simulate the PBL with a uniform underlying surface under various stratifications very well, and it is consistent with the existing field observations and numerical simulations. (2) The characteristic dimensions of eddies in the CBL, NBL, and SBL with a uniform underlying surface are about $Z_i, h/2$, and $h/4$, respectirely (here Z_i is the height of the CBL and h is the height of the NBL and SBL). (3) Streaky structures appear in the lower part of the NBL. A net pattern forms in the CBL due to the horizontal eddy. The small streaky structure parallel to the wind direction appears in the lower part of the SBL. (4) Due to the adoption of the anisotropy TKE closure model, the resolved part of the physical variables increases and

the SGS part decreases. So more energetic, higher frequency eddies appear, and the precondition of LES is better met.

The comparison and analysis of an LES on the UBL show the following: (1) The result from an LES of the UBL with a proposed formula of the drag coefficient is consistent and comparable with that from wind tunnel experiments and an urban subdomain scale model. (2) Due to the effect by urban buildings, the wind velocity near the canopy is decreased, turbulence is intensified, TKE, variance, and momentum flux are increased, the momentum and heat flux at the top of the PBL are increased, and the development of the PBL is quickened. (3) The height of the roughness sublayer (RS) of actual city buildings is the maximum building height (1.5–3 times the mean building height), and a constant flux layer (CFL) exists in the lower part of the UBL.

It can be concluded that an LES of the UBL can resolve two key problems in the urban parameterization for mesoscale meteorological models: parameter specification and model validation. And LES has special advantages in the study of the UBL. So research on the UBL using LES is necessary.

Acknowledgments. The research was supported by the National Natural Science Foundation of China under Grant Nos. 40333027 and 40075004.

REFERENCES

Brown, M. J., 2000: Urban parameterizations for mesoscale meteorological models. *Mesoscale Atmospheric Dispersion*. Z. Boybeyi, Ed., Wessex Institute of Technology Press, Boston, 193–255.

Brown, M. J., and M. Williams, 1998: An urban canopy parameterization for mesoscale meteorological models. *AMS 2nd Urban Environment Symposium*, Albuquerque, NM, 10A.1, 1–4.

Cai, X-M., 1999: Large-eddy simulation of the convective boundary layer over an idealized patchy urban surface. *Quart. J. Roy. Meteor. Soc.*, **125**, 1427–1444.

Deardorff, J. W., 1980: Stratocumulus-capped mixed layers derived from a three-dimensional model. *Bound.-Layer Meteor.*, **18**, 495–527.

Ge Xiaozhen, 1994: *The Numerical Method in Atmospheric Sciences.* Nanjing University Press, Nanjing, 472pp. (in Chinese)

Kosović, B., and J. A. Curry, 2000: A large eddy simulation study of a quasi-steady, stably stratified atmospheric boundary layer. *J. Atmos. Sci.*, **57**, 1052–1068.

Martilli, A., A. Clappier, and M. W. Rotach, 2002: An urban surface exchange parameterization for mesoscale models. *Bound.-Layer Meteor.*, **104**, 261–304.

Mason, P. J., and D. J. Thomson, 1992: Stochastic backscatter in large-eddy simulations of boundary layers. *J. Fluid Mech.*, **242**, 51–78.

Miao Shiguang, and Jiang Weimei, 2004: Large eddy simulation of turbulent flow in forest canopy and forest boundary layer. *Chinese Journal of Geophysics*. (in Chinese, in print)

Miao Shiguang, Jiang Weimei, Wang Xiaoyun, Zhang Ning, Ji Congping, and Li Ju, 2002: Numerical simulation of meteorology and pollutant diffusion in urban subdomain. *Acta Scientiae Circumstantiae*, **22**, 478–483. (in Chinese)

Moeng, C-H., 1984: A large-eddy-simulation model for the study of planetary boundary-layer turbulence. *J. Atmos. Sci.*, **41**, 2052–2062.

Moeng, C-H., and P. P. Sullivan, 1994: A comparison of shear- and buoyancy-driven planetary boundary layer flows.*J. Atmos. Sci.*, **51**, 999–1022.

Nieuwstadt, F. T. M., 1984: The turbulent structure of the stable, nocturnal boundary layer. *J. Atmos. Sci.*, **41**, 2202–2216.

Ouyang Yan, Jiang Weimei, and Miao Shiguang, 2003: Experimental study in wind tunnel on field of air flows and pollutant dispersion in the urban subdomain. *Journal of Nanjing University* (*Natural Sciences*), **39**, 770–780. (in Chinese)

Raupach, M. R., 1992: Drag and drag partition on rough surfaces. *Bound.-Layer Meteor.*, **60**, 375–395.

Rotach, M. W., 2001: Simulation of urban-scale dispersion using a Lagrangian stochastic dispersion model. *Bound.-Layer Meteor.*, **99**, 379–410.

Roth, M., 2000: Review of atmospheric turbulence over cities. *Quart. J. Roy. Meteor. Soc.*, **126**, 941–990.

Schmidt, H., and U. Schumann, 1989: Coherent structure of the convective boundary layer derived from large eddy simulation. *J. Fluid Mech.*, **200**, 511–562.

Sullivan, P. P., J. C. McWilliams, and C-H. Moeng, 1994: A subgrid-scale model for large eddy simulation of planetary boundary-layer flows. *Bound.-Layer Meteor.*, **71**, 247–276.

Wyngaard, J. C., 1984: Large-eddy simulation–Guidelines for its application to planetary boundary layer research. The U.S. Army Research Office, AD-A146 381, 69pp.

Zhang Hanxin, and Shen Mengyu, 2003: *Computational Fluid Dynamics—The principle and Application of Difference Method*. National Defence Industry Press, Beijing, 289pp.